APL Photonics

RESEARCH ARTICLE | APRIL 18 2025

Low background fluorescence 3D-printed micro-lens for imaging of vulnerable atherosclerotic plaques

Rouyan Chen ; Florian Rothermel ; Robert Fitridge ; Christina A. Bursill ; Peter J. Psaltis; Harald Giessen; Alois Herkommer ; Robert A. McLaughlin ; Andrea Toulouse ; Jiawen Li

APL Photonics 10, 040805 (2025)
https://doi.org/10.1063/5.0247546

Low background fluorescence 3D-printed micro-lens for imaging of vulnerable atherosclerotic plaques

Cite as: APL Photon. 10, 040805 (2025); doi: 10.1063/5.0247546
Submitted: 7 November 2024 • Accepted: 27 March 2025 •
Published Online: 18 April 2025

Rouyan Chen,[1,2,3] Florian Rothermel,[4,5] Robert Fitridge,[6,7] Christina A. Bursill,[3,7] Peter J. Psaltis,[3,7,8] Harald Giessen,[5,9] Alois Herkommer,[4,5] Robert A. McLaughlin,[2,7] Andrea Toulouse,[4,5,a)] and Jiawen Li[1,2,a)]

AFFILIATIONS

[1] School of Electrical and Mechanical Engineering, University of Adelaide, Adelaide, SA 5005, Australia
[2] Institute for Photonics and Advanced Sensing, University of Adelaide, Adelaide, SA 5005, Australia
[3] Lifelong Health Theme, South Australian Health and Medical Research Institute (SAHMRI), Adelaide, SA 5000, Australia
[4] Institute of Applied Optics (ITO), University of Stuttgart, 70569 Stuttgart, Germany
[5] Research Center SCoPE, University of Stuttgart, 70569 Stuttgart, Germany
[6] Vascular and Endovascular Service, Central Adelaide Local Health Network, Adelaide, SA 5000, Australia
[7] Faculty of Health and Medical Sciences, University of Adelaide, Adelaide, SA 5005, Australia
[8] Department of Cardiology, Central Adelaide Local Health Network, Adelaide, SA 5000, Australia
[9] 4th Physics Institute, University of Stuttgart, 70569 Stuttgart, Germany

[a)] **Authors to whom correspondence should be addressed:** andrea.toulouse@ito.uni-stuttgart.de and Jiawen.li01@adelaide.edu.au

ABSTRACT

Vulnerable atherosclerotic plaques, which are prone to rupture, can result in life-threatening events, such as strokes and heart attacks. These plaques are distinguished by features including a large necrotic core, macrophage infiltration, spotty calcification, intraplaque hemorrhage, and a thin fibrous cap. While current intravascular optical coherence tomography (OCT) is capable of visualizing structural characteristics of plaques, such as the fibrous cap thickness, it has limitations in reliably identifying vulnerable plaques. Previous studies have demonstrated that intraplaque hemorrhage and oxidized lipids in the necrotic core and of vulnerable plaques generate autofluorescence when excited at 633 nm. Our team has designed and developed a 3D-printed micro-lens probe that utilizes a photoresist, IP-Visio, with low background fluorescence. This photoresist is ideal for autofluorescence detection of vulnerable plaques in the visible range, without the need for externally injected fluorophores. The micro-lens on the tip of a double clad fiber has two apertures that address the threefold purpose of our probe: OCT imaging, fluorescence excitation, and fluorescence collection by a combination of focal and afocal optical design. With this dual aperture design, we have achieved in capturing the weak autofluorescence signals and high-resolution OCT images from *ex vivo* human carotid plaques, using the IP-Visio micro-lens intravascular probe. We validated these imaging results with histology and a commercial benchtop fluorescence imaging system. This work paves the way for the wider application of 3D-printed micro-lenses for multimodal OCT and fluorescence imaging in the visible and near-infrared range, especially with intravascular or endoscopic devices.

INTRODUCTION

Atherosclerosis is a chronic disease that is characterized by the accumulation of cholesterol-rich, inflamed plaques in the walls of arteries. The most common complication associated with these plaques is the rupture of the overlying fibrous cap, which accounts for up to 70% of fatal acute myocardial infarction and sudden coronary deaths.[1] Plaques that are more prone to rupture can be referred to as vulnerable plaques. These plaques have hallmark features, such as a thin fibrous cap, high lipid burden, large necrotic core, infiltration of inflammatory cells, intraplaque hemorrhage, and spotty calcification.[1] The detection of vulnerable plaque features is important to guide risk stratification and treatment strategies to prevent catastrophic cardiovascular events.

Plaque imaging can be used to detect and study the natural history of vulnerable plaques and their responsiveness to therapy.[2,3] Single modality imaging devices used in contemporary clinical practice include intravascular ultrasound and optical coherence tomography (OCT), which can visualize different morphological features of plaque. However, they are currently limited by a low positive predictive value for identifying plaques that will go on to cause ischemic events.[4,5] This is partly because they do not incorporate biomolecular information that is indicative of the dynamic processes leading to plaque complications, such as plaque rupture.[1]

Biomolecular information of atherosclerotic plaques can be studied using technologies such as fluorescence even without the use of exogenous fluorescent markers.[6] Various components of plaque, including elastin, collagen, lipids, and intraplaque hemorrhage, all exhibit intrinsic fluorescence signatures, also referred to as autofluorescence.[7,8] Previous studies have identified that autofluorescence, excited at 633 nm, was detected in plaques with necrotic cores, originating from oxidized lipids and heme degradation products from intraplaque hemorrhage.[9,10] This autofluorescence signal was found to be in the red to near-infrared region. Using these longer wavelengths, in preference to the ultraviolet (UV) range, improves the contrast between stable and vulnerable plaques, as the light can penetrate deeper into the tissue. An attractive aspect of acquiring biomolecular information through autofluorescence, rather than using exogenous contrast agents, is that it avoids the need for injecting dyes into the body, which can lead to adverse events, such as immune responses,[11] and requires regulatory approval for adoption into clinical practice.[12]

Multimodal OCT and fluorescence imaging devices have been developed to integrate biomolecular information together with morphological features.[13,14] This can be achieved through a single double clad fiber and a single micro-lens.[14–17] 3D printing of a micro-lens can provide increased design freedom, for instance, splitting the aperture and combining OCT and fluorescence imaging to ensure sufficient sensitivity to detect weak autofluorescence signals. This was previously explored by our team as we developed a novel lens-in-lens design[13] with a high numerical aperture (NA) for fluorescence collection. The present work represents a different implementation of our lens-in-lens concept. While we concentrated on achieving a high NA in our previous study, here, we aimed for a twofold focal/afocal collection design, both concentrated on the fluorescence excitation region. Since the excitation region is relatively far away from the center of our micro-probe, fluorescence originating from this point can naturally only transmit our probe's aperture at small angles. Therefore, we aimed for focal fluorescence collection through the inner aperture (in line with the excitation) and afocal fluorescence collection through the outer aperture, i.e., a minimized angular spreading while overall achieving an improved concentration on the region of interest compared to the high NA case.

In general, dual modality imaging has the potential to improve the prediction rate of plaque rupture, as the OCT can provide high-resolution information about the morphology of plaque, and the fluorescence provides additional biomolecular data.[4] However, our previously employed photoresist IP-S, which is commonly utilized for 3D printing of micro-lenses, was unfit to analyze the 633 nm-excited autofluorescence of vulnerable human plaques,[9,10,18,19] as it is fluorescent under the visible range.[20] Therefore, a lower background fluorescence photoresist is needed for the autofluorescence measurement in the visible range.

IP-Visio (Nanoscribe GmbH & Co KG, Germany), a biocompatible photoresist material with very low background fluorescence in the visible spectrum,[20] is a suitable printing material for the 3D printed lens. Using this material would mean that the background fluorescence from the lens will not confound the autofluorescence detected from the human tissue, allowing more accurate capture of the true autofluorescence signal from the tissue sample.

In this paper, we explore the use of this low background fluorescence photoresist, IP-Visio, to 3D print a micro-lens for a miniaturized OCT and (auto-)fluorescence fiber-optic probe. We first adapted our lens-in-lens optical design for OCT imaging and fluorescence detection from a distant (1 mm) excitation region to enable imaging of human carotid plaques *ex vivo*. In a second step, we improved our mechanical design to enable fabrication on the tip of an optical fiber with IP-Visio. Fluorescence results acquired with our miniaturized fiber-optic probe were validated against wide-field fluorescence images acquired with an in vivo imaging system (IVIS) and histological sections imaged by fluorescence microscopy, while morphological features identified in the OCT were validated against co-located hematoxylin and eosin (H&E) histological sections. Biomolecular information of the atherosclerotic plaques was detected by our low background fluorescence 3D printed micro-lens imaging probe.

METHODS

Optical lens design

To enable the high-sensitivity detection of fluorescence signals in small arteries, the 3D-printed micro-lens was designed to enable intravascular OCT imaging and autofluorescence collection at a working distance of 1 mm in a side-viewing arrangement (Fig. 1). Note that the fluorescence detection sensitivity drops as the vessel radius increases and that a modified design would be required for high-sensitivity detection in larger vessels. The total internal reflection (TIR) mirror surface and the front surface of the micro-lens were implemented using biconic surface types to correct for aberrations of the catheter sheath due to the break of symmetry. To maximize autofluorescence collection from the excitation region, we split the front aperture of the lens to focal (inner) and afocal (outer) parts. The inner (focal) aperture focuses the fluorescence light from the excitation point to the core of the DCF. The outer (afocal) aperture serves to redistribute light emitted from the excitation point

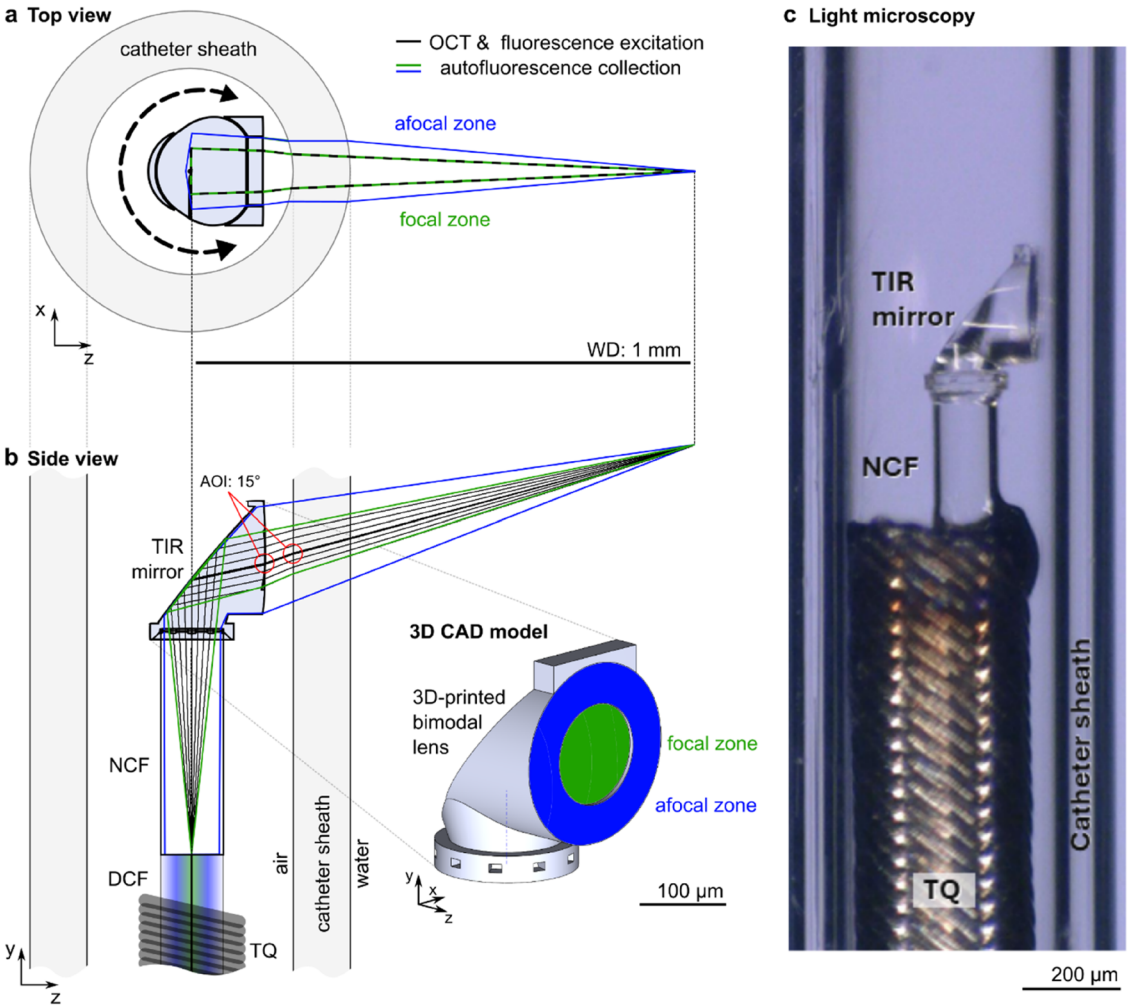

FIG. 1. Multimodal OCT+autofluorescence probe. [(a) and (b)] schematics of the multimodal probe design. A 3D-printed micro-lens is assembled on top of an NCF piece attached to a DCF. The probe is mechanically stabilized by a torque coil and can be rotated within a catheter sheath. The core of the DCF transports the OCT signal (1300 nm) and the fluorescence excitation (633 nm). The first cladding collects autofluorescence (710 nm design wavelength). The 3D-printed micro-lens is split into two apertures, i.e., a focal zone in the center (green) and an afocal ring aperture (blue). The focal zone creates diffraction limited foci for OCT and fluorescence excitation. Both the focal zone and the afocal zone serve to collect autofluorescence from within the excitation region into the core and inner cladding of the DCF. (c) Light microscopy image of the assembled probe inside a catheter sheath. OCT: optical coherence tomography, NCF: no core fiber, DCF: double clad fiber, TIR: total internal reflection, TQ: torque coil, WD: working distance, and AOI: angle of incidence.

across the inner cladding of the DCF. A comparison of focal, afocal, and the high NA design case is provided in the supplementary material, Fig. S1, showing that an afocal design can improve fluorescence collection by the inner cladding of the collection fiber. The chief ray angle at the micro-lens front surface and the catheter sheath is fixed to 15° to suppress ghost images at these high refractive index contrast surfaces.

Optical designs were optimized using Zemax OpticStudio (Ansys, Canonsburg, PA, USA). OCT (1300 nm, config. 1 in Fig. 2), fluorescence excitation (633 nm, config. 2 in Fig. 2), and fluorescence collection (710 nm, config. 3 and 4 in Fig. 2) beam paths were implemented via a multi-configuration, assuming one or multiple fields emitting from the core and the inner cladding, respectively (see the supplementary material, Fig. S2). This uses the specified numerical aperture of the DCF core (NA 0.12) and the inner cladding (NA 0.2). Configurations 1, 2, and 3 were optimized for the inner aperture for a minimum root mean square (RMS) spot (focal) of fields originating from the DCF core (configurations 1 and 2) and the inner cladding (configuration 3). Configuration 4 was optimized for the outer aperture for best collimation per field point (afocal), originating from the inner cladding. The inner aperture and the outer aperture of the front surface have diameters of 120 and 200 µm, respectively. For OCT and fluorescence excitation, our simulation predicts diffraction limited performance with airy radii of 12.8 and

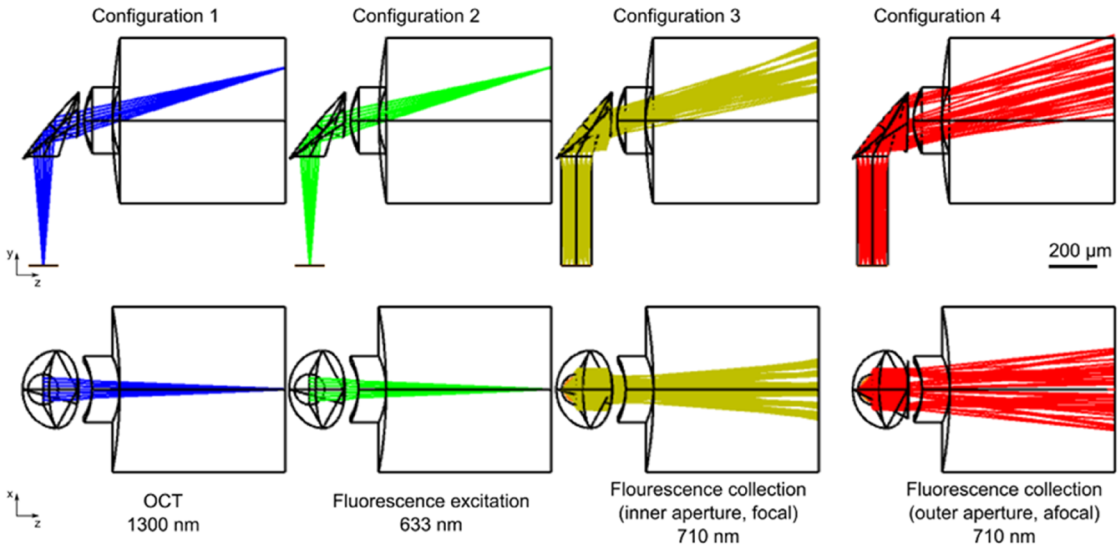

FIG. 2. Optimization results for the four different configurations considered in our OCT and fluorescence micro-lens.

6.1 µm, respectively. Optimized coefficients for all biconic surfaces are given in the supplementary material, Table S3.

Mechanical design and fabrication

The mechanical 3D computer-aided design (CAD) model of the probe was designed in SolidWorks (Dassault Systèmes SE, France). The optical surfaces were imported from Zemax OpticStudio and mechanically connected through solid material. As the IP-Visio material barely generates background fluorescence, which is often needed to directly detect the interface when printing a micro-lens onto a fiber,[21] the 3D printed micro-lens was printed onto a glass substrate coated with indium-tin-oxide and then assembled onto an optical fiber. A mechanical guide was designed to facilitate this assembling process. The 3D model was exported as a printable STL-file that was sliced and hatched with 0.1 and 0.15 µm, respectively. The micro-lenses were printed using the Photonic Professional GT2 (Nanoscribe GmbH, Germany) in dip-in configuration with a 40× microscope objective (Plan-Apochromat 40X/1.4 Oil DIC M27, Carl Zeiss Microscopy Deutschland GmbH, Germany). For the IP-Visio probes, we used a galvo scanning speed of 50 mm s^{-1}, a laser power of 27.5 mW for the first 200 slices, and a laser power of 32.5 mW for the rest. To compare the performance of IP-Visio with IP-S, the material that has been commonly used for 3D printing micro-lenses,[21,22] we also fabricated the same micro-lens design using IP-S. For the IP-S probes, a galvo scanning speed of 100 mm s^{-1} and a consistent laser power of 25 mW were used. After printing, all samples were developed in propylene glycol methyl ether acetate (PGMEA) for 12 min and afterward rinsed with isopropanol for 2 min. It should be noted that IP-Visio requires higher light doses and simultaneously has a narrower processing window of polymerization compared to IP-S. Simply increasing the writing laser power poses the risk of undesired bubble formation, as slices close to the substrate interface receive higher doses due to back reflection. The laser power therefore had to be adapted to the axial position of the slices.

A micromanipulation setup was used for the assembly of the 3D-printed micro-lenses and fibers. Liquid photoresist (either IP-Visio or IP-S) was applied to the fiber tip and followed by joining the aligned fiber with the 3D-printed micro-lens through the mechanical guide incorporated in the 3D-printed structure. Using UV illumination, the photoresist was cured, and the 3D-printed micro-lens adhered to the fiber.

Multimodal OCT and fluorescence system setup

The imaging system setup (Fig. 3) was described in our previous study,[23] although the laser and filters have been modified to better suit the autofluorescence excitation and collection. In particular, the fluorescence excitation laser has a center wavelength at 633 nm (Matchbox 0633 L-13 A, Integrated Optics, UAB). A 635 ± 10 nm bandpass filter (FLH635-10, Thorlabs Inc., USA) was used to narrow the laser spectrum, and a 700 nm long pass filter (FELH0700, Thorlabs, USA) was used to filter out the excitation laser. Furthermore, a low background fluorescence double clad fiber coupler module (DC1300LE2, Castor Optics Inc., Canada) was utilized to further reduce the background fluorescence from the system. The DCF coupler unit is directly fiber coupled to the optical fiber probe using a fiber connector/angled physical contact (FC/APC) mating sleeve. The optical fiber probe is then fitted into a bespoke rotation/translation stage to acquire radial pullback scans. The system uses a counter-rotation scheme, in which the probe is rotated to acquire a full radial scan and then counter-rotated prior to the next step of the pullback. This approach avoids the need for a rotary coupler, significantly simplifying efficient acquisition of the fluorescence and OCT signals.

The imaging probe is made using a long piece of double clad fiber (>200 cm, DCF13, Thorlabs Inc., USA), terminated with

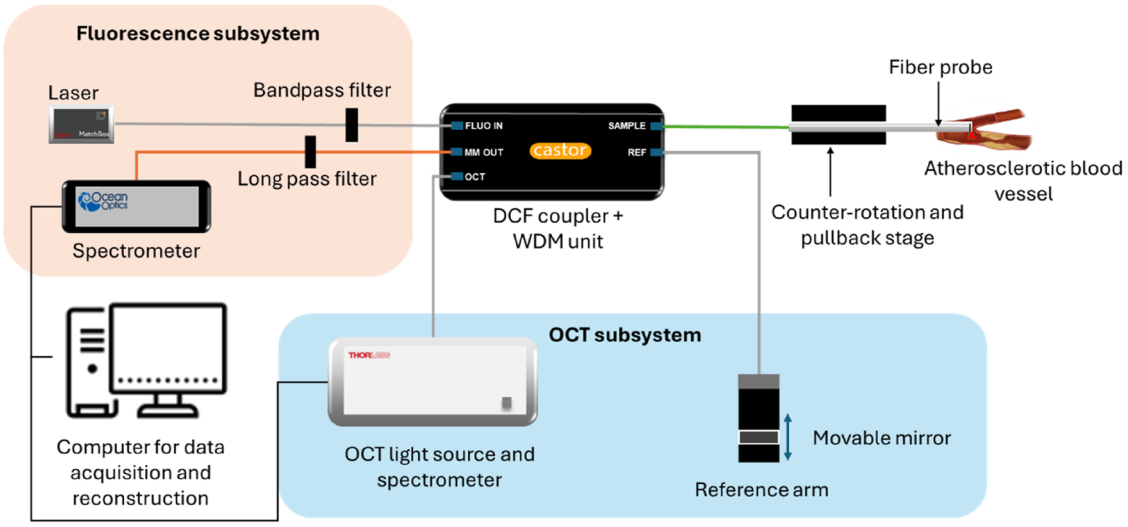

FIG. 3. Schematic of the multimodal OCT and fluorescence system; the OCT sub-system (blue region) and the fluorescence sub-system (orange region) are combined using a double-clad fiber (DCF) coupler module, which contains a DCF coupler and a wavelength division multiplexer (WDM) unit. Gray colored line: single mode fiber; green colored line: DCF; orange colored line: multimode fiber. Note that the (green) DCF continues to the distal end of the probe but is obscured here once it enters the torque coil and catheter sheath.

450 μm of no core fiber (NCF125, Success Prime Corporation, Taiwan) and a 3D printed micro-lens glued onto the end. The optical fiber probe was then fitted within a metal coil (ACTONE, ASAHI Intecc Co., Ltd., Japan) and enclosed within a plastic catheter sheath (material: fluorinated ethylene propylene, 410 μm internal diameter, 635 μm outer diameter; ZEUS Inc., USA; refractive index = 1.33).

Ex vivo imaging of human carotid plaques

All human experiments and procedures were approved by the Central Adelaide Local Health Network Human Research Ethics Committee (Ref: 15120) at the Royal Adelaide Hospital, Australia, and the study was conducted in accordance with the principles of the Declaration of Helsinki. Human carotid plaques were collected from endarterectomy procedures for patients presenting with a stroke or transient ischemic attack at the Royal Adelaide Hospital. Informed consent was received from all patients before the procedure. The resected carotid plaque was then imaged in the laboratory within 2 hours of the procedure. Prior to intravascular imaging, the sample was imaged inside an IVIS (IVIS® Lumina XRMS, 640 nm excitation and 710 nm + emission) for 2D fluorescence measurement. Next, the carotid plaque was imaged using the imaging probe with either the IP-Visio or IP-S printed micro-lens at 5 mW for fluorescence excitation. A light source power of 7.5 mW was used for the OCT system. Note that a cylindrical coordinate system comprised of radial distance (r), axial length (z), and azimuth angle (θ) is used throughout this manuscript to explain the rotation and pullback for imaging. For each 360° rotation, 1600 OCT radial scans were generated, 32 fluorescence spectra were acquired, and the axial step is 20 μm in between each rotation. With the current imaging setup, the counter-rotation and pullback stage can perform one revolution in 2 s, and the pullback speed is 5.5 s per 20 μm step, for both OCT and fluorescence measurements. Compared to the clinically available OCT system, the current multimodal OCT and fluorescence device is slower, due to the use of a spectrometer for fluorescence measurement. The spectra are useful for distinguishing the true autofluorescence from system background fluorescence.[24] During the imaging process, phosphate buffered saline was applied to the tissue to retain its moisture. After imaging, the specimen was decalcified in a 10% ethylenediaminetetraacetic acid (EDTA) solution for one week and then embedded in an optimal cutting temperature medium for fresh frozen cryosectioning. The carotid plaque was sectioned at 5 μm sections. Prior to histological analysis, the tissues were fixed in a 2% paraformaldehyde phosphate buffered saline solution for 10 min. 2% paraformaldehyde is a commonly used fixative, which prevents the tissue from degrading to maintain the cell morphology and tissue structure. A previous study has shown that autofluorescence was preserved after using this fixing agent.[9]

Image processing

Fluorescence images overlayed onto the OCT images were processed such that each radial scan is represented by the summation of the intensities of the fluorescence spectrum over the wavelength range of 700–1130 nm. This wavelength (1130 nm) was the extent of our spectrometer, and we chose to acquire all available data rather than setting an empirical upper threshold wavelength.

3D reconstruction of the atherosclerotic plaque was achieved using Amira Software (Zuse Institute Berlin and Thermo Fisher Scientific, USA) for 3D volume rendering of the OCT images acquired using the IP-Visio lens fiber probe.

A 2D heat map was generated from the fluorescence spectra obtained using the IP-Visio imaging probe using a custom MATLAB program (MathWorks, USA). The 2D heat map represents the fluorescence detected over the entire pullback, with the vertical axis indicating the azimuthal angle of the probe and the horizontal axis of the heat map aligned with the pullback direction indexed by the axial distance (20 μm) moved between each rotation.

Histological analysis

Histology was performed on the sectioned specimen; stains include H&E for general plaque morphology and 4′,6-diamidino-2-phenylindole (DAPI) for cell nuclei. H&E stained sectioned were digitized using a digital slide scanner (NanoZoomer, Hamamatsu Photonics, Japan). DAPI stained sections were imaged using a slide scanner (ZEISS Axio Scan.Z1 Slide Scanner, Carl Zeiss AG, Germany), with 385 nm for the DAPI channel and 633 nm for the autofluorescence of the human tissue.

The histology images were co-registered with the intravascular OCT and fluorescence images by correlating the distance from the start of the scan pullback for both the OCT scan and histological section and by identifying matching anatomical landmarks.

RESULTS

Comparison between IP-Visio and IP-S micro-lens

Ex vivo OCT and fluorescence images were acquired for human carotid plaques, using probes fabricated with IP-Visio and IP-S micro-lenses [Figs. 4(a), 4(b), 4(e), and 4(f)], where Figs. 4(a) and 4(b) are taken from a cross section with lower tissue autofluorescence, and Figs. 4(e) and 4(f) are taken from a cross section with

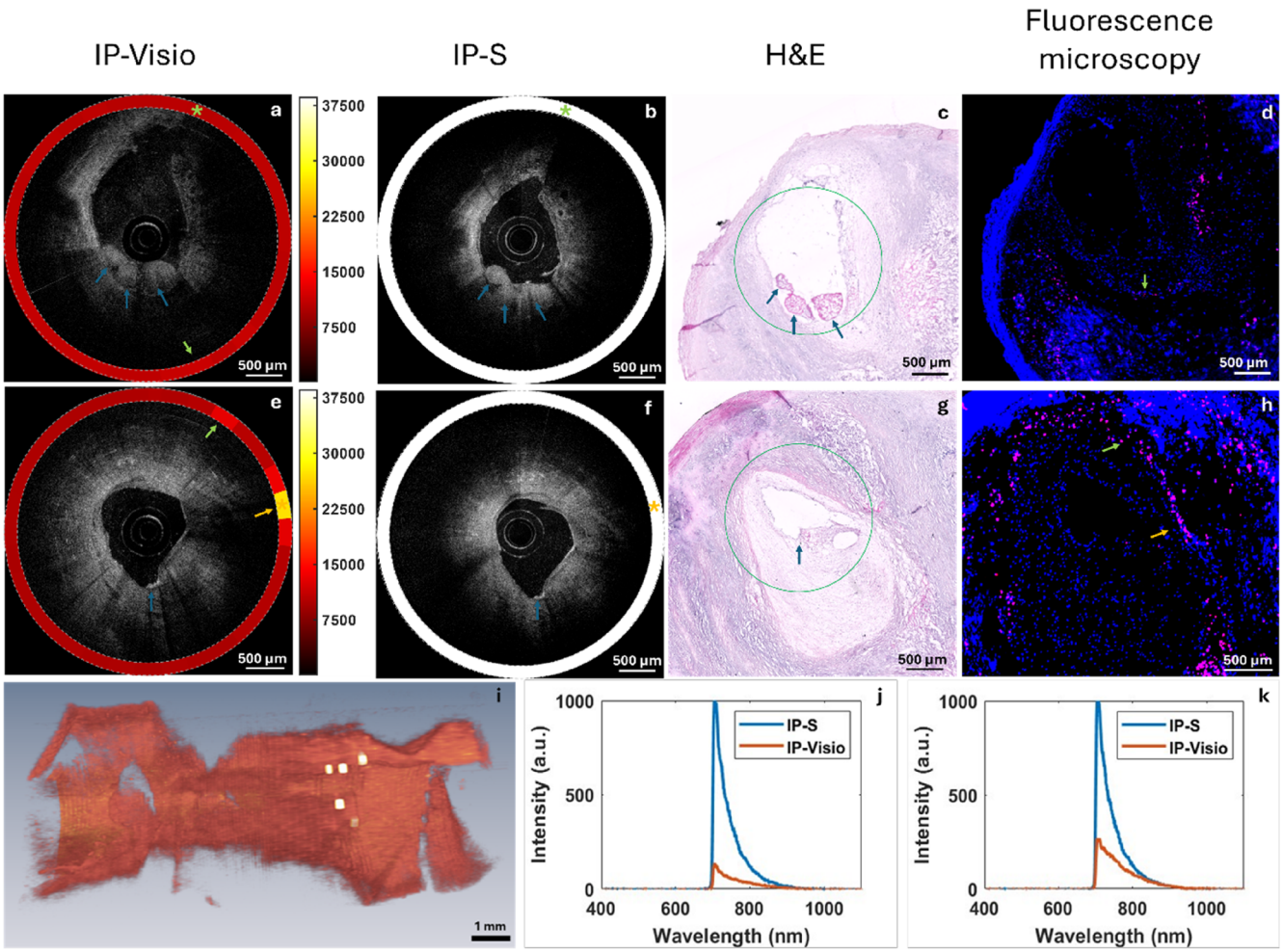

FIG. 4. Comparison between IP-Visio and IP-S micro-lens in imaging a human plaque. (a) Example of OCT and fluorescence images acquired using the IP-Visio micro-lens, showing low autofluorescence. (b) OCT and fluorescence images of the same region in (a) acquired using the IP-S micro-lens. (c) H&E histological section co-located with (a) and (b); the green circle indicates the region of the plaque that was within the imaging range of the probe. (d) Fluorescence microscopy image co-located with (a) and (b); blue: DAPI (cell nuclei) and magenta: autofluorescence. (e) OCT and fluorescence images acquired using the IP-Visio micro-lens, showing high autofluorescence from a different section of the pullback scan. (f) OCT and fluorescence images of the same region in (e) acquired using the IP-S micro-lens. (g) H&E histology section co-located with (e) and (f); the green circle indicates the region of the plaque that was within the imaging range of the probe. (h) Fluorescence microscopy image co-located with (e) and (f); blue: DAPI (cell nuclei) and magenta: autofluorescence. (i) Cutaway view of the 3D reconstruction of the carotid plaque from OCT and autofluorescence images acquired with the IP-Visio micro-lens. (j) Background fluorescence spectra obtained from the radial scan highlighted with green asterisks in (a) and (b). (k) Tissue autofluorescence spectra obtained from the radial scan highlighted with yellow asterisks in (e) and (f). The green arrows indicate areas with low autofluorescence detection by the imaging probe; the yellow arrows indicate areas with high autofluorescence; the blue arrows represent the features that were used to correlate the OCT images with H&E.

higher tissue autofluorescence. OCT images are the central grayscale images in Figs. 4(a), 4(b), 4(e), and 4(f), and the intravascular fluorescence is displayed as a color-coded ring overlayed outside of the OCT images. The OCT imaging performance, in terms of resolution and penetration depth, is comparable with what has previously been reported with a state-of-art intravascular OCT device.[25] These OCT images are matched with H&E stained sections in Figs. 4(c) and 4(g). Figure 4(a) is acquired from a cross section of the plaque where the autofluorescence is low (indicated by the green arrow). This corresponds to the fluorescence microscopy image in Fig. 4(d) (fluorescence shown in magenta, indicated by green arrow). Figure 4(e) is acquired from a cross section of the plaque where a high autofluorescence signal was observed (yellow arrow). This is validated against the fluorescence microscopy image in Fig. 4(h) (fluorescence in magenta with yellow arrow). Corresponding to the H&E images, the fluorescence signals in Figs. 4(d) and 4(h) appear within the necrotic core region of the carotid plaque; this is visualized by the increased acellular lipid area (small white regions) on the H&E. The contrast of the blue color (DAPI stain) on the fluorescence images [Figs. 4(d) and 4(h)] was increased to better visualize the cell nuclei in the regions that were imaged, and this has caused saturation in other areas on the section with more cells. Note that there are lower autofluorescence signals from adjacent areas [green arrow in Fig. 4(e) and 4(h)], where the lower measured autofluorescence may have caused by the increased distance from the tissue to the probe. The false-positive artifact of saturated high fluorescence intensity observed for the IP-S micro-lens is due to the strong fluorescence of the IP-S material itself under visible light.[20] Variation in the fluorescence intensity across different azimuthal angles is illustrated in the supplementary material, Fig. S4. 3D reconstruction of the OCT images obtained with the IP-Visio micro-lens was performed using Amira and is shown in Fig. 4(i), showing overlayed fluorescence hotspots in white.

A comparison of the IP-Visio and IP-S micro-lenses demonstrated that both micro-lenses provide similar OCT image quality; the signal-to-ratio was evaluated to be 100.88 dB for IP-Visio micro-lens and 99.96 dB for IP-S micro-lens (see the supplementary material, Fig. S5). However, as shown in Fig. 4(j), the fluorescence spectra acquired are very different. This spectrum was taken from ~15° on Fig. 4(a) (indicated by the green asterisk), where no autofluorescence signal was detected. This was validated through the lack of autofluorescence detected from the fluorescence microscopy image in the co-located region [Fig. 4(d)]. The peak fluorescence intensity from IP-S is ~10 times higher than that for IP-Visio micro-lens under the 633 nm laser excitation wavelength [Fig. 4(j)], due to the high background fluorescence of the IP-S material. The spectrum in Fig. 4(j) (IP-Visio spectrum) depicts the background fluorescence of the system. The source of this background fluorescence signal comes from components in the system, which include the double clad fiber coupler (DCFC) and the DCF. Several modifications have been made to minimize residual background fluorescence in the system,[24] i.e., utilizing a DCFC with low autofluorescence components and minimal fiber probe length possible. Figure 4(k) shows the fluorescence spectrum of measurements indicated by yellow asterisks in Figs. 4(e) and 4(f), showing an area of high tissue autofluorescence. The IP-Visio spectrum in Fig. 4(k) reveals a higher autofluorescence intensity measurement than that in Fig. 4(j), correlating with the increased autofluorescence in the tissue. In contrast, the IP-S fluorescence spectrum in both Figs. 4(j) and 4(k) remains the same, indicative of high background fluorescence in the IP-S dominating measurements from the tissue.

Ex vivo imaging of human carotid plaques

A macro-scale image of a human carotid plaque is shown in Fig. 5(a). Figure 5(b) illustrates the fluorescence acquired using IVIS,

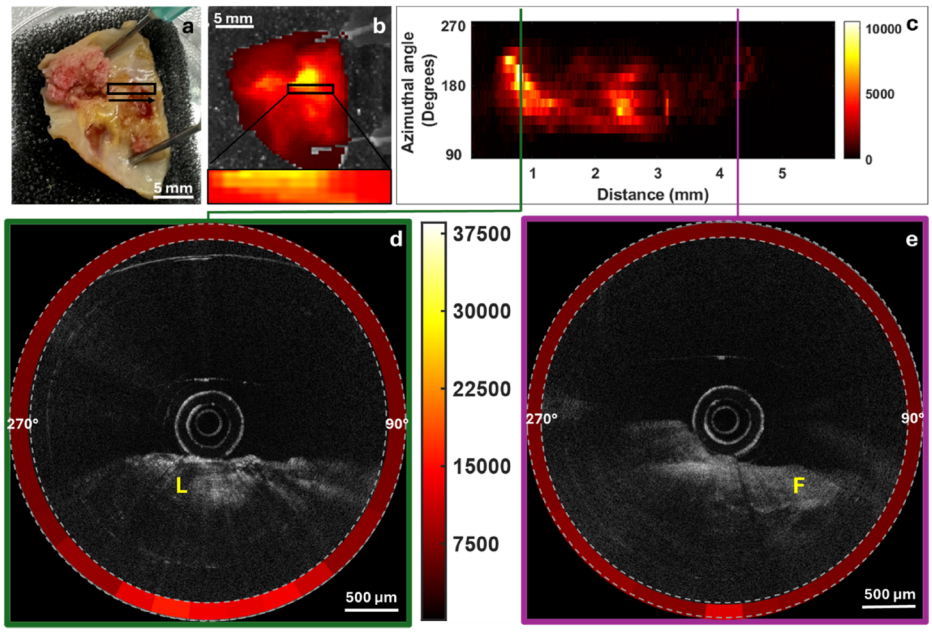

FIG. 5. IVIS imaging of human plaque compared to intravascular imaging using the fiber probe with an IP-Visio micro-lens. (a) Macro-scale image of a human carotid plaque; the black arrow indicates the direction of the scan using the IP-Visio micro-lens. (b) IVIS image of the plaque with overlayed fluorescence; the fluorescence hotspot is shown in yellow. (c) 2D fluorescence heatmap of the region in the black box in (a) and (b), in the direction shown in (a); fluorescence was acquired using the imaging probe with an IP-Visio micro-lens. [(d) and (e)] Examples of multimodal OCT and fluorescence images at different locations along the pull back: (d) earlier in the pull back where there was strong autofluorescence (L: lipidic region) and (e) further into the pull back where weaker autofluorescence was observed (F: fibrotic region).

which can be observed grossly where the fluorescence hotspots correspond to the tissue sample. Using these hotspots as a guide, the plaques were then imaged using a fiber probe with the IP-Visio micro-lens for OCT and autofluorescence imaging. A 2D heat map was created from the fluorescence measurements acquired by the 3D-printed IP-Visio micro-lens, depicted in Fig. 5(c). As 32 fluorescence spectral measurements are acquired over each 360° rotation of the intravascular imaging, a 2D heat map was generated to better compare with the IVIS scan acquired before intravascular scanning. Due to the surgical technique used, the excised plaques have a vertical cut in the middle. Thus, only 90° to 270° of fluorescence represents where the probe is in contact with the tissue sample [Figs. 5(d) and 5(e)].

The trend of the fluorescence intensity was similarly illustrated across both fluorescence imaging techniques, where higher fluorescence was observed at the start of the scan [OCT frame 25, Fig. 5(c)] in comparison with the IVIS scan [left of the magnified inset Fig. 5(b)] and decreases after passing the fluorescence hotspot [OCT frame 155, Fig. 5(c)]. However, the fluorescence heat map generated by the 3D-printed micro-lens is somewhat different from the IVIS fluorescence image. This is due to the different mechanisms by which fluorescence images are acquired between these two techniques.

Plaque microstructures were visible in the OCT image [gray color central images in Figs. 5(d) and 5(e)], showing both lipidic [Fig. 5(d)] and fibrotic regions [Fig. 5(e)] according to the consensus standards for image interpretation.[26] Fluorescence signals [outer colorful rings in Figs. 5(d) and 5(e)] correspond to plaque features [90°–270° in Figs. 5(d) and 5(e)], with different compositional features associated with different levels in fluorescence intensity. For example, higher fluorescence intensity co-localized lipid-rich plaque, as seen in OCT [135°–225° in Fig. 5(d)].

DISCUSSION

This study examined a 3D printing photoresist material, IP-Visio, to fabricate a micro-lens for an intravascular OCT and fluorescence imaging probe to detect autofluorescence of atherosclerotic plaques because of its low background fluorescence. The design of the micro-lens allows the easy fabrication and assembling of the micro-lens onto an optical fiber. It also realizes the autofluorescence collection by dividing the front aperture of the micro-lens into focal and afocal zones for distant imaging. In future, splitting the aperture into more than two zones to embed additional functionality or further improved collection efficiency could be investigated. The working distance of the lens was also tailored to 1 mm, as an extension to our earlier study, which had been limited to imaging smaller vessel diameters (with a 0.5 mm fluorescence focal length).[13] The fluorescence obtained using the IP-Visio micro-lens allowed us to identify autofluorescence signal from an atherosclerotic plaque, validated with fluorescence microscopy and IVIS. High fluorescence signals were detected with the IP-S micro-lens, and this was due to the fluorescence of the material itself. We note that the quality of OCT imaging was comparable between these two different lens materials, as both reveal plaque morphology that matches features identified in the H&E sections. Importantly, the fluorescence signals acquired by the IP-Visio micro-lens compared favorably with IVIS, as the probe had a higher resolution than the benchtop IVIS system. The probe has an excitation airy radius of 6.1 μm, whereas the pixel resolution of the IVIS is 50 μm.[27] The fluorescence channel resolution of our probe during intravascular imaging is dependent on the scattering of the carotid tissue. Rather than optimizing the fluorescence resolution, our design has incorporated an afocal zone to improve fluorescence collection, utilizing the entire inner cladding of the DCF.

Taken together, these results indicate that it is not adequate to use an IP-S micro-lens to capture the autofluorescence of human carotid plaques when excited using a 633 nm wavelength. Since many biological molecules are fluorescent in the visible spectrum,[27] if the desired application is for fluorescence imaging in the visible spectrum at a shorter wavelength, such as in the airways at 445 nm,[14,28] the background fluorescence of the IP-S lens will impact the fluorescence collection of the sample more dramatically.[20] In comparison with IP-S, the use of IP-Visio complicates direct printing onto optical fiber facets, as autofluorescence of the resin was often required for precise manual interface finding. This was circumvented here by first printing the micro-lenses onto glass substrates, followed by post-process assembly with the optical fiber. Despite involving more process steps, this method is more efficient for batch production of fiber assembled probes.

Previous research has reported that in carotid atherosclerotic plaques, the presence of intraplaque hemorrhage was associated with stroke and coronary heart disease, whereas the presence of lipid-rich necrotic core and calcification were not significantly linked to stroke or coronary heart disease.[29] The current study focuses on identifying autofluorescence from vulnerable carotid plaques, as they were more readily accessible. Further analysis is required to identify specific plaque components in vulnerable plaques that lead to clinical complications.

In conclusion, a micro-lens fabricated from IP-Visio photoresist has been effectively employed to image carotid plaques. The micro-lens provides high resolution imaging of anatomical features from the OCT. In addition, the micro-lens has enabled successful detection of the weak autofluorescence which is characteristic of vulnerable plaques, offering valuable biomolecular information for plaque assessment.

SUPPLEMENTARY MATERIAL

See the supplementary material for details on the (1) non-sequential Zemax model for validating the design intent of the micro-lens, (2) simulated field points and the performance of the probe, (3) biconic surface descriptions and optimized coefficients, (4) quantitative plots of fluorescence variations across the radial scan, and (5) signal to noise ratio measurement of IP-Visio and IP-S micro-lenses.

ACKNOWLEDGMENTS

We thank Dr. Albert Kota, Dr. Christina Popovic, Dr. Shabnam Torabiardakani, Dr. Kay Hon, Dr. Guilherme Pena, Dr. Joanne Tan, Dr. Simon Thiele, Mr. Marco Wende, Mr. Bryden Quirk, Dr. Alok Kushwaha, Mr. Rodney Kirk, Ms. Claudia Imiolczyk, Ms. Yujia Kong, and Dr. Lei Xiang for fruitful discussions and their help in

the collection the human carotid plaques, design and manufacturing of the fiber probe, developing of the imaging software, assisting with the imaging and transportation of the micro-lenses, and assisting with the intravascular imaging. The authors wish to extend their sincere thanks to the individuals who generously donated their tissues to support the progress of education and research. The authors also acknowledge the instruments and expertise of Microscopy Australia at Adelaide Microscopy, the University of Adelaide, enabled by NCRIS, university, and state government support. This research was supported by an Australian Government Research Training Program (RTP) Scholarship.

The authors were supported by the National Health and Medical Research Council (NHMRC) Development Grant No. 2022337, Ideas Grant No. 2001646, and Investigator Grant No. 2008462), the Heart Foundation Future Leader Fellowship (Grant Nos. 105608 and 106656), the hospital research foundation project Grant No. 2022-CP-IDMH-014-83100, Australia–Germany Joint Research Co-operation Scheme (UA-DAAD), Baden-Württemberg-Stiftung (Opterial, Elite Program for Postdocs), European Research Council (Advanced Grant Complexplas, PoC Grant 3DPrintedOptics), Bundesministerium für Bildung und Forschung (3DPrintedOptics, Integrated3Dprint, QR.X, QR.N, DAAD 57701620), Deutsche Forschungsgemeinschaft (DFG, German Research Foundation, Grant Nos. 431314977/GRK2642 and 461765984), HORIZON EUROPE European Innovation Council (IV-Lab 101115545), Carl-Zeiss Foundation (EndoPrint3D, QPhoton), and the University of Stuttgart (Terra Incognita).

AUTHOR DECLARATIONS

Conflict of Interest

P.J.P. has received research support from Abbott Vascular, Amgen, and Biotronik; consulting fees from Amgen, Esperion, Eli Lilly, Novartis, Novo Nordisk, and Sanofi; and speaker honoraria from Amgen, AstraZeneca, Bayer, Boehringer Ingelheim, Merck Schering-Plough, Pfizer, Novartis, Novo Nordisk, and Sanofi. He also serves as an unpaid board director of Corcillum Systems Ltd. R.A.M. is a co-founder and the Director of Miniprobes Pty Ltd., a company that develops optical imaging systems. Miniprobes Pty Ltd. did not contribute to or participate in this study. J.L. is the founder and Director of Theia Medical Pty Ltd., a company that develops medical imaging devices. Theia Medical Pty Ltd. did not contribute to or participate in this study. H.G. and A.H. are co-founders of PrintOptix GmbH, a company that develops 3D printed optics. H.G. is the inventor on a patent related to this work (international publication Nos. WO2017059960A1 and DE102015012980B4). The remaining authors declare no competing interest.

Ethics Approval

All human experiments and procedures were approved by the Central Adelaide Local Health Network Human Research Ethics Committee (CALHN HREC) and CALHN Research Governance (Ref: 15120) at the Royal Adelaide Hospital, Australia. Informed consent was obtained from all participants.

Author Contributions

Rouyan Chen: Conceptualization (equal); Data curation (equal); Formal analysis (equal); Investigation (equal); Methodology (equal); Validation (equal); Visualization (equal); Writing – original draft (equal); Writing – review & editing (equal). **Florian Rothermel**: Investigation (equal); Methodology (equal); Writing – review & editing (equal). **Robert Fitridge**: Funding acquisition (supporting); Methodology (supporting); Resources (equal); Supervision (equal); Writing – review & editing (equal). **Christina A. Bursill**: Methodology (supporting); Supervision (equal); Writing – review & editing (equal). **Peter J. Psaltis**: Funding acquisition (equal); Methodology (supporting); Writing – review & editing (equal). **Harald Giessen**: Funding acquisition (equal); Methodology (supporting); Writing – review & editing (equal). **Alois Herkommer**: Funding acquisition (equal); Methodology (supporting); Supervision (supporting); Writing – review & editing (equal). **Robert A. McLaughlin**: Resources (equal); Supervision (equal); Writing – review & editing (equal). **Andrea Toulouse**: Conceptualization (equal); Funding acquisition (equal); Investigation (equal); Methodology (equal); Supervision (equal); Writing – review & editing (equal). **Jiawen Li**: Conceptualization (equal); Funding acquisition (equal); Investigation (equal); Methodology (equal); Supervision (equal); Writing – review & editing (equal).

DATA AVAILABILITY

The data that support the findings of this study are available from the corresponding authors upon reasonable request.

REFERENCES

[1] M. Naghavi *et al.*, "From vulnerable plaque to vulnerable patient," Circulation **108**, 1664–1672 (2003).
[2] N. J. Montarello, A. J. Nelson, J. Verjans, S. J. Nicholls, and P. J. Psaltis, "The role of intracoronary imaging in translational research," Cardiovasc. Diagn. Ther. **10**, 1480–1507 (2020).
[3] P. J. Psaltis *et al.*, "Optical coherence tomography assessment of the impact of colchicine on non-culprit coronary plaque composition after myocardial infarction," Cardiovasc. Res. **00**, cvae191 (published online, 2024).
[4] J. Li *et al.*, "Multimodality intravascular imaging of high-risk coronary plaque," JACC: Cardiovasc. Imaging **15**, 145–159 (2022).
[5] K. Fujii *et al.*, "Accuracy of OCT, grayscale IVUS, and their combination for the diagnosis of coronary TCFA: An ex vivo validation study," JACC: Cardiovasc. Imaging **8**, 451–460 (2015).
[6] M. J. Mitchinson, D. C. Hothersall, P. N. Brooks, and C. Y. De Burbure, "The distribution of ceroid in human atherosclerosis," J. Pathol. **145**, 177–183 (1985).
[7] Y. Uchida *et al.*, "Detection of vulnerable coronary plaques by color fluorescent angioscopy," JACC: Cardiovasc. Imaging **3**, 398–408 (2010).
[8] N. M. Htun *et al.*, "Near-infrared autofluorescence induced by intraplaque hemorrhage and heme degradation as marker for high-risk atherosclerotic plaques," Nat. Commun. **8**, 75 (2017).
[9] M. S. Albaghdadi *et al.*, "Near-infrared autofluorescence in atherosclerosis associates with ceroid and is generated by oxidized lipid-induced oxidative stress," Arterioscler., Thromb., Vasc. Biol. **41**, e385–e398 (2021).
[10] M. Kunio *et al.*, "Histopathological correlation of near infrared autofluorescence in human cadaver coronary arteries," Atherosclerosis **344**, 31–39 (2022).
[11] J. Meira, M. L. Marques, F. Falcao-Reis, E. Rebelo Gomes, and A. Carneiro, "Immediate reactions to fluorescein and indocyanine green in retinal angiography: Review of literature and proposal for patient's evaluation," Clin. Ophthalmol. **14**, 171–178 (2020).
[12] B. W. Pogue, E. L. Rosenthal, S. Achilefu, and G. M. van Dam, "Perspective review of what is needed for molecular-specific fluorescence-guided surgery," J. Biomed. Opt. **23**, 1–9 (2018).

[13]J. Li *et al.*, "3D-Printed micro lens-in-lens for in vivo multimodal microendoscopy," Small **18**, 2107032 (2022).
[14]H. Pahlevaninezhad *et al.*, "Endoscopic high-resolution autofluorescence imaging and OCT of pulmonary vascular networks," Opt. Lett. **41**(14), 3209–3212 (2016).
[15]L. Scolaro, D. Lorenser, W.-J. Madore, R. W. Kirk, A. S. Kramer, G. C. Yeoh, N. Godbout, D. D. Sampson, C. Boudoux, and R. A. McLaughlin, "Molecular imaging needles: Dual-modality optical coherence tomography and fluorescence imaging of labeled antibodies deep in tissue," Biomed. Opt. Express **6**, 1767–1781 (2015).
[16]S. Liang *et al.*, "Intravascular atherosclerotic imaging with combined fluorescence and optical coherence tomography probe based on a double-clad fiber combiner," J. Biomed. Opt. **17**(7), 070501 (2012).
[17]H. Yoo *et al.*, "Intra-arterial catheter for simultaneous microstructural and molecular imaging *in vivo*," Nat. Med. **17**, 1680–1684 (2011).
[18]H. Wang *et al.*, "Ex vivo catheter-based imaging of coronary atherosclerosis using multimodality OCT and NIRAF excited at 633 nm," Biomed. Opt. Express **6**, 1363–1375 (2015).
[19]G. J. Ughi *et al.*, "Clinical characterization of coronary atherosclerosis with dual-modality OCT and near-infrared autofluorescence imaging," JACC: Cardiovasc. Imaging **9**, 1304–1314 (2016).
[20]M. Schmid, D. Ludescher, and H. Giessen, "Optical properties of photoresists for femtosecond 3D printing: Refractive index, extinction, luminescence-dose dependence, aging, heat treatment and comparison between 1-photon and 2-photon exposure," Opt. Mater. Express **9**(12), 4564–4577 (2019).
[21]J. Li *et al.*, "Ultrathin monolithic 3D printed optical coherence tomography endoscopy for preclinical and clinical use," Light: Sci. Appl. **9**, 124 (2020).
[22]T. Gissibl, S. Thiele, A. Herkommer, and H. Giessen, "Two-photon direct laser writing of ultracompact multi-lens objectives," Nat. Photonics **10**, 554–560 (2016).
[23]R. Chen *et al.*, "Detection of atherosclerotic plaques with HDL-like porphyrin nanoparticles using an intravascular dual-modality optical coherence tomography and fluorescence system," Sci. Rep. **14**, 12359 (2024).
[24]L. Xiang *et al.*, "Identification and removal of system-induced autofluorescence in miniaturized fiber-optic fluorescence endoscopes," arXiv:2503.07921 [physics.optics] (2025).
[25]B. E. Bouma, M. Villiger, K. Otsuka, and W.-Y. Oh, "Intravascular optical coherence tomography [Invited]," Biomed. Opt. Express **8**, 2660–2686 (2017).
[26]G. J. Tearney *et al.*, "Consensus standards for acquisition, measurement, and reporting of intravascular optical coherence tomography studies," J. Am. Coll. Cardiol. **59**, 1058–1072 (2012).
[27]A. C. Croce and G. Bottiroli, "Autofluorescence spectroscopy and imaging: A tool for biomedical research and diagnosis," Eur. J. Histochem. **58**(4), 2461 (2014).
[28]H. Pahlevaninezhad *et al.*, "A high-efficiency fiber-based imaging system for co-registered autofluorescence and optical coherence tomography," Biomed. Opt. Express **5**, 2978–2987 (2014).
[29]D. Bos *et al.*, "Atherosclerotic carotid plaque composition and incident stroke and coronary events," J. Am. Coll. Cardiol. **77**, 1426–1435 (2021).